# Graphene plasmon propagation on corrugated silicon substrates

Xiang-Tian Kong, Bing Bai, and Qing Dai*

*National Center for Nanoscience and Technology, Beijing 100190, China*
*Corresponding author: daiq@nanoctr.cn*

The scheme of graphene on a silicon substrate is potentially compatible to the microelectronic technology. But the maintained plasmons have considerable ohmic loss because of silicon's large permittivity. We introduce air grooves in the silicon surface to reduce the optical thickness of substrate and hence decrease the propagation loss. The properties of graphene plasmons on the corrugated substrates are numerically investigated, in terms of the photon frequency and the geometrical parameters of the corrugated layer, considering both ohmic loss and scattering loss. The plasmons propagation lengths for the corrugated substrates can exceed twice of those for flat silicon in a broadband in mid-infrared. This study may be useful for designing of compact mid-infrared waveguides based on graphene for future photonic integrated circuits.  © 2014 Optical Society of America

*OCIS codes:*   (240.6680) Surface plasmons; (230.7370) Waveguides; (050.6624) Subwavelength structures.

http://dx.doi.org/10.1364/OL.40.000001

When mid-infrared photons coherently oscillate with the collective motions of the charge carriers in doped graphene, tightly confined plasmon polaritons are excited [1–4]. Graphene plasmons (GPs) have much greater momenta than the free space photons exciting them, enabling manipulation of mid-infrared lights at sub-micron scales [3–6]. Owing to the tight confinement of GPs and the one-atom thickness of graphene, the optical properties of the guided plasmons, including the wave propagation and energy loss, are considerably affected by the dielectric environment [7,8]. For instance, GPs of energies above 0.1 eV are strongly hybridized with the surface polar phonons of silica in the typical experimental configuration of graphene on a silica substrate [5,6], yielding inelastic scattering and extra damping of the plasmons [5–7]. Thereby, substrate materials play a critical role in routing and manipulating of GPs.

Use of a nonpolar substrate, such as silicon [9] and diamond-like carbon [5], can avoid the hybridization between GPs and substrate phonons. In particular, graphene-silicon heterostructures are potentially compatible to the mature microelectronic technology [9–11]. In addition, silicon is transparent in a broad range in the infrared domain (its extinction coefficient is less than $10^{-3}$ for photon energies below 1.1 eV [12]). Several applications of GPs using the graphene-on-silicon configuration have already been demonstrated, such as excitation of GPs by diffractive grating etched in silicon [13] and tunable Bragg filter [14]. However, limited by the fundamental trade-off between the mode confinement and the propagation loss, the GP propagation is seriously degraded due to the extremely small mode volume resulted from the large permittivity of silicon.

In this report, we propose to lower down the propagation loss of the plasmons by replacing the flat silicon substrate with a corrugated one. The corrugated layer is optically thinner than the bulk silicon due to the introduced air grooves, yielding increased mode volume and hence reduced ohmic loss. When the corrugated layer is fine enough (e.g., when the groove array period is one twentieth of the GP wavelength) along the wave propagation direction, the scattering loss can be negligibly small, and the corrugated region can be viewed as an effective anisotropic layer according to the effective medium theory (note that the limit case of GPs on half-infinite uniaxial substrates has been studied in [15]). However, such fine structures are often not easy to fabricate for today's state of the art. And grooves with finite widths bring light scattering, which still lacks an in-depth study. Here we focus on GP propagation on corrugated substrates with finite groove widths, taking into account the scattering loss from the grooves.

Figure 1(a) shows the geometry and notations of the proposed plasmonic waveguide consisting of graphene on a corrugated silicon substrate. The groove array period, $f$, is assumed to be several times less than the GP wavelength, $\lambda_{GP}$. For short array period limit (SAPL, $f/\lambda_{GP} \to 0$), the optical responses of the corrugated layer are equivalent to those of an anisotropic material layer [Fig. 1(b)] with the nonzero elements of the relative permittivity tensor given by [16]
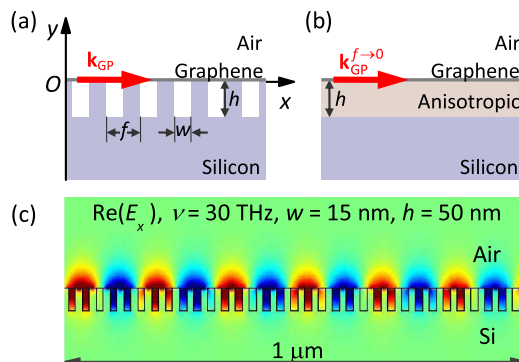


Fig. 1.   (a) Configuration of plasmonic waveguide consisting of a graphene sheet on silicon penetrated by an array of air grooves. (b) Effective structure of short array period limit (SAPL, $f/\lambda_{GP} \to 0$), where the anisotropic layer has the same thickness as the air grooves, with its permittivity given by Eq. (1). (c) Snapshot of longitude electric field at frequency of 30 THz, assuming $w = 15$ nm, $h = 50$ nm, $f = 2w$ and graphene Fermi level of 0.4 eV.

$$\epsilon_{xx} = 1/[(w/f)/\epsilon_{\mathrm{air}} + (1 - w/f)/\epsilon_{\mathrm{Si}}],$$
$$\epsilon_{yy} = \epsilon_{zz} = (w/f) \cdot \epsilon_{\mathrm{air}} + (1 - w/f) \cdot \epsilon_{\mathrm{Si}}. \qquad (1)$$

Here $\epsilon_{\mathrm{air}}$ and $\epsilon_{\mathrm{Si}}$ are relative permittivities of air and silicon, respectively. The effective permittivity depends only on the groove width-to-period ratio, $w/f$. For convenience, we assume $w/f = 1/2$ throughout this report.

Finite element method is used to calculate the plasmon behaviors in the structures shown in Figs. 1(a) and 1(b). The guided wave is excited at the leftmost boundary of the calculation domain and propagates along the graphene sheet. Graphene's surface conductivity is given by the Kubo formula (see graphene modeling details in [17]), assuming a moderate graphene Fermi level of 0.4 eV, and charge mobility of $10,000 \ \mathrm{cm}^2/(\mathrm{V} \cdot \mathrm{s})$ (Ref. [18]). The substrate is assumed to be highly transparent intrinsic silicon, whose refractive index is given by the Herzberger-type formula that is fitted from empirical data [12], $n_{\mathrm{Si}} = 3.419 + 0.1232L + 0.02655L^2$, where $L = 1/(\lambda_0^2 - 0.028)$, and $\lambda_0$ is free space wavelength in micron unit. Note that here we ignore the ohmic loss from substrate, which however has to be considered for heavily doped silicon [19].

Figure 1(c) shows a typical snapshot of the longitude electric field of the guided plasmon at frequency of $\nu = 30$ THz, with geometrical parameters of $w = 15$ nm and $h = 50$ nm. Stable propagating GP mode is sustained in this configuration, although the corrugated layer has a coarse groove period ($f \sim \lambda_{\mathrm{GP}}/5$). The GP on the corrugated silicon experiences alternative regions of air–graphene–air–silicon and air–graphene–silicon, resulting in a nonsinusoidal field profile along the propagation direction, especially in the substrate. Nevertheless, the field profile above the graphene sheet is almost a (damped) sinusoid along the propagation direction.

We describe a guided GP mode by its effective refractive index, $n_{\mathrm{eff}}$, which is the propagation constant, $k_{\mathrm{GP}}$, normalized by the free-space wavevector, $k_0$. To obtain $n_{\mathrm{eff}}$, discrete $E_x$ data at $y = 80$ nm are extracted and fitted by the damped oscillation function of the type $E_x = A \exp(-k_i x) \exp(i k_r x)$. Thus the GP propagation constant is given by $k_{\mathrm{GP}} = k_r + i k_i$ and $n_{\mathrm{eff}} = k_{\mathrm{GP}}/k_0$. Next, we first discuss the dispersive properties of GPs on the corrugated substrate with fixed guide geometries, and then demonstrate how these properties are affected by the geometrical parameters.

Figures 2(a) and 2(b) show the numerically calculated frequency-dependent effective refractive index (real and imaginary parts, respectively) of GPs on corrugated substrates, as well as that of GPs on flat silicon and the scattering-free configuration of SAPL (denoted by $w = 0$) for comparison. To ensure the correctness of the numerical model, we also exploit the analytical formula that is deduced from Maxwell equations [1] to calculate the curve of $n_{\mathrm{eff}}$ versus $\nu$ for GPs on flat silicon surface (not shown), which presents no observable difference from the numerically simulated one, suggesting high accuracy of our numerical method.

The real part of the effective refractive index, $\mathrm{Re}(n_{\mathrm{eff}})$, monotonously raises as the photon frequency increases for both the flat and corrugated substrates. Thus GP wavelength monotonously decreases according to
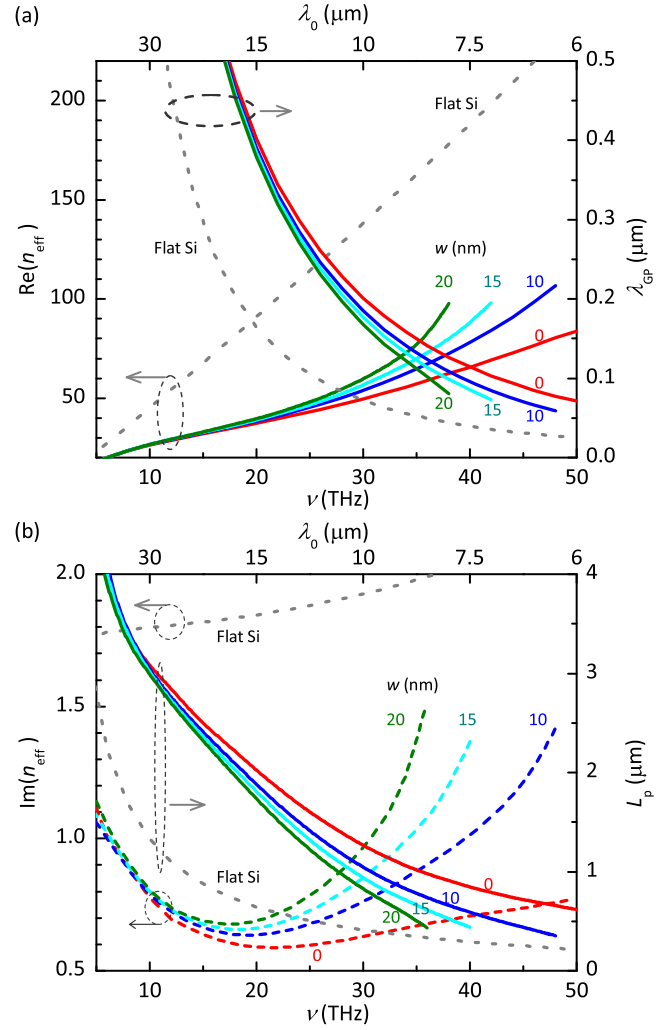


Fig. 2. Dispersion of GPs on silicon, corrugated silicon ($w = 10, 15, 20$ nm) and substrate of SAPL (denoted by $w = 0$). Thickness of corrugated layer is $h = 100$ nm. (a) Real part of effective refractive index (left axis) and GP wavelength (right axis) with respect to photon frequency. (b) Imaginary part of effective refractive index (left axis) and propagation length (right axis) with respect to photon frequency.

$\lambda_{\mathrm{GP}} = \lambda_0/\mathrm{Re}(n_{\mathrm{eff}})$, and the mode volume, which is determined by $\lambda_{\mathrm{GP}}$ [1], also decreases. In contrast, the imaginary part of the effective refractive index, $\mathrm{Im}(n_{\mathrm{eff}})$, has very different dispersion behaviors for a flat substrate and corrugated substrates. Unlike the monotonously raised $\mathrm{Im}(n_{\mathrm{eff}})$ of GPs on flat silicon, $\mathrm{Im}(n_{\mathrm{eff}})$ of GPs on the corrugated substrates, including the one assuming SAPL, first falls and then raises as the photon frequency increases. Nonetheless, the propagation length, defined by $L_p = 1/2k_0 \mathrm{Im}(n_{\mathrm{eff}})$, falls monotonously for both the flat and the corrugated substrates. GPs on the corrugated substrate of SAPL have less values of $\mathrm{Re}(n_{\mathrm{eff}})$ and less $\mathrm{Im}(n_{\mathrm{eff}})$ compared with those on flat silicon, and hence possess longer wavelengths and longer propagation lengths. For finite groove array periods, both the real and the imaginary parts of $n_{\mathrm{eff}}$ are greater than those of the SAPL configuration. As the photon frequency increases, when the groove array periods are eventually comparable to $\lambda_{\mathrm{GP}}/2$, the scattering losses become

extremely large, and GPs cease to propagate. Before reaching the cutoff frequencies, GPs on the corrugated substrates propagate longer than that on flat silicon [Fig. 2(b)]. For example, for substrates with $w = 15$ nm and $h = 100$ nm, $L_p$ exceeds twice of that of flat silicon for $\nu < 35$ THz.

The deviation between $n_{\text{eff}}$ of GPs on corrugated substrates with finite groove array periods and that of GPs on the SAPL configuration originates from the GPs scattering from the grooves. For the scattering-free SAPL configuration, GP propagation constant $k_{\text{GP}}^{f \to 0}$ is simply determined by the permittivity and thickness of the effective anisotropic layer. Whereas for the corrugated substrate with a finite array period, the fields penetrate much deeper in the air grooves than in silicon, resulting in impedance mismatch between the fields in the air–graphene–air–silicon and air-graphene-silicon regions, and generating unavoidable back-scattered field.

Consider that a corrugated substrate with a finite groove array period evolves from the one with SAPL as the air groove array period widens from infinitesimal to a finite value. We suppose during this evolution the combined momentum of the scattered fields, i.e., the forward and backward guided fields and that scattered off to the free space, keeps a constant as long as the normalized groove array period, $f/\lambda_{\text{GP}}$, is small. Due to the momentum conservation, the forward GP wavevector, $\text{Re}(k_{\text{GP}})$, is greater than $\text{Re}(k_{\text{GP}}^{f \to 0})$, when the back-scattered field exists. Moreover, the normalized groove array period raises as the photon frequency increases, yielding elevated momentum of the back-scattered field, thus widening the deviation of $\text{Re}(n_{\text{eff}})$ of the waveguide with a corrugated substrate from the limit value of $\text{Re}(k_{\text{GP}}^{f \to 0})/k_0$ [Fig. 2(a)]. Meanwhile, the scattered field results in greater $\text{Im}(n_{\text{eff}})$ of the waveguide with a corrugated substrate than that with SAPL. And when increasing the photon frequency, the deviation of $\text{Im}(n_{\text{eff}})$ from the limit value $\text{Im}(k_{\text{GP}}^{f \to 0})/k_0$ widens due to the elevated field scattering [Fig. 2(b)]. Herein, the difference between $n_{\text{eff}}$ and the limit of $k_{\text{GP}}^{f \to 0}/k_0$ can be considered as a measurement of the scattered field.

The scattered field varies with the geometrical parameters of the corrugated layer. Figure 3 shows the effective refractive index and propagation length of GPs on the corrugated substrates in terms of the groove width at fixed frequencies, with fixed corrugated layer thicknesses (see caption for parameter values). The normalized groove array period $f/\lambda_{\text{GP}}$ is less than 0.3 within the groove width ranges in Fig. 3. The real part of $n_{\text{eff}}$ almost linearly raises when widening the air grooves [(a), (d)], indicating that the amount of the back-scattered field linearly grows with the enlarging groove width for small values of $f/\lambda_{\text{GP}}$. Because of the scattering loss, $\text{Im}(n_{\text{eff}})$ also linearly raises when widening the grooves [(b), (e)], and correspondingly $L_p$ linearly decreases [(c), (f)]. The growth of $\text{Re}(n_{\text{eff}})$ with respect to $w$ is insensitive to the corrugated layer thickness. But it increases with increasing photon frequency, because the scattering of GPs is stronger for a higher frequency. Due to the same reason, the decreasing rate of $L_p$ with respect to $w$ also increases when increasing the frequency. When the frequency increases from 10
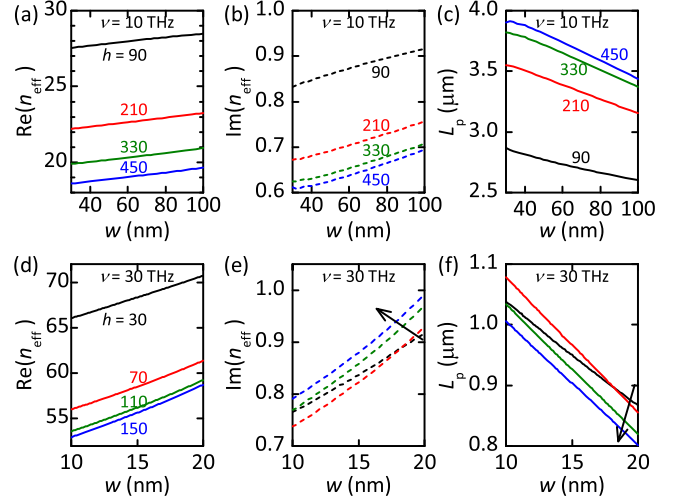


Fig. 3. Effective refractive index $n_{\text{eff}}$ and propagation length $L_p$ in terms of air groove width $w$, with fixed air groove thicknesses $h$. (a) and (d) Real part of $n_{\text{eff}}$. (b) and (e) Imaginary part of $n_{\text{eff}}$. (c) and (f) Propagation length. In (a)–(c), $\nu = 10$ THz. In (d)–(f), $\nu = 30$ THz. Along the arrows in (e) and (f), $h = 30, 70, 110, 150$ nm.

to 30 THz, the value of $\partial \text{Re}(n_{\text{eff}})/\partial w$ grows from $\sim 0.015$ nm$^{-1}$ to $\sim 0.55$ nm$^{-1}$, and $|\partial L_p/\partial w|$ varies from $\sim 6$ to $\sim 20$.

Figure 4 shows the effective refractive index and propagation length of GPs on the corrugated substrates in terms of the corrugated layer thickness with fixed groove widths at fixed photon frequencies (see caption for parameters). As the corrugated layer becomes thicker, $\text{Re}(n_{\text{eff}})$ decreases [(a), (c)], thus the modes become less tightly confined. This is because the mean refractive index of the environment experienced by GPs lowers as the optically thinner layer becomes thicker. When the corrugated layer thickness exceeds
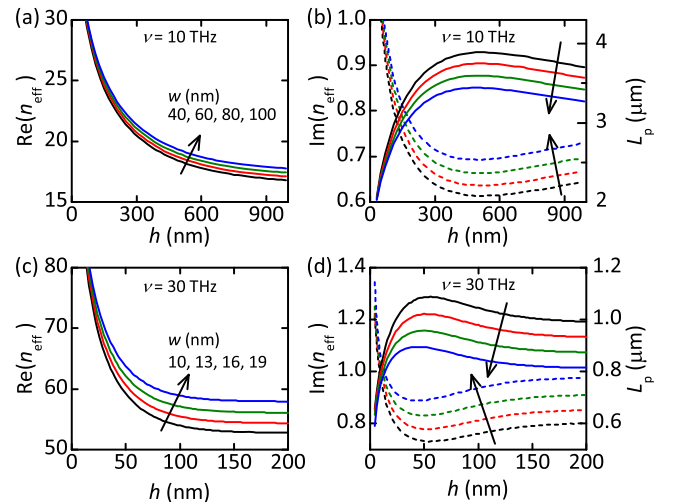


Fig. 4. Effective refractive index and propagation length in terms of corrugated layer thickness, with fixed air groove widths. (a) and (c) Real part of $n_{\text{eff}}$. (b) and (d) Imaginary part of $n_{\text{eff}}$ (dashed) and propagation length (solid). In (a) and (b), $\nu = 10$ THz, $w = 40, 60, 80, 100$ nm along the arrows. In (c) and (d), $\nu = 30$ THz, $w = 10, 13, 16, 19$ nm along the arrows.

the penetration depth of GPs in the substrate, the curves of $Re(n_{eff})$ go flat as $h$ increases.

In contrast, when enlarging $h$, $Im(n_{eff})$ first decreases and then increases, and hence $L_p$ first rises and then falls [(b), (d)]. This is because the propagation loss is affected by two simultaneous processes with opposite consequences when thickening the corrugated layer. First, the reduced field confinement lowers down the ohmic loss; but secondly, the thickened corrugated layer elevates the scattering loss. The reduced amount of ohmic loss is greater than the raised scattering loss for thin corrugated layers, but the scattering loss grows as the corrugated layer thickens and eventually exceeds the reduced ohmic loss.

The two processes balance at the minimum of $Im(n_{eff})$ in Figs. 4(b) and 4(d), where GPs acquire maximum propagation lengths. The corrugated layer thickness for maximum $L_p$ slightly decreases with enlarging groove width, and decreases also with the increasing frequency. When the frequency increases from 10 to 30 THz, the $L_p$ maximum position falls from $h \simeq 500$ nm to $h \simeq 50$ nm. Note that unlike the curves for the finite groove widths, $Im(n_{eff})$ of the scattering-free SAPL waveguide decreases monotonously when thickening the anisotropic layer.

In conclusion, the dispersion, damping and scattering of the guided GPs on corrugated silicon substrates have been numerically studied. In general, the propagation of GPs on a corrugated substrate suffers from both the ohmic loss and the scattering loss. Compared with the scattering-free SAPL configuration, GP momentum is elevated by the back-scattered field from the corrugated layer, resulting in tighter mode confinement and higher ohmic loss. The ohmic loss grows when widening the air grooves, but falls when thickening the corrugated layer. Whereas the scattering loss raises when enlarging either the groove width or the corrugated layer thickness. As a result of the two distinct loss mechanisms, the propagation length decreases monotonously when widening the air grooves, but first raises and then falls when thickening the corrugated layer. This study is also helpful in understanding other types of surface electromagnetic waves on non-conductive corrugated substrates, and may be useful for future on-chip photonic applications.

## References

1. M. Jablan, H. Buljan, and M. Soljacic, Phys. Rev. B **80**, 245435 (2009).
2. A. Y. Nikitin, F. Guinea, F. J. Garcia-Vidal, and L. Martin-Moreno, Phys. Rev. B **84**, 195446 (2011).
3. J. Chen, M. Badioli, P. Alonso-Gonzalez, S. Thongrattanasiri, F. Huth, J. Osmond, M. Spasenovic, A. Centeno, A. Pesquera, P. Godignon, A. Zurutuza Elorza, N. Camara, F. J. G. de Abajo, R. Hillenbrand, and F. H. L. Koppens, Nature **487**, 77 (2012).
4. Z. Fei, A. S. Rodin, G. O. Andreev, W. Bao, A. S. McLeod, M. Wagner, L. M. Zhang, Z. Zhao, M. Thiemens, G. Dominguez, M. M. Fogler, A. H. C. Neto, C. N. Lau, F. Keilmann, and D. N. Basov, Nature **487**, 82 (2012).
5. H. Yan, T. Low, W. Zhu, Y. Wu, M. Freitag, X. Li, F. Guinea, P. Avouris, and F. Xia, Nat. Photonics **7**, 394 (2013).
6. V. W. Brar, M. S. Jang, M. Sherrott, J. J. Lopez, and H. A. Atwater, Nano Lett. **13**, 2541 (2013).
7. E. H. Hwang, R. Sensarma, and S. Das Sarma, Phys. Rev. B **82**, 195406 (2010).
8. M. Freitag, T. Low, L. Martin-Moreno, W. Zhu, F. Guinea, and P. Avouris, ACS Nano **8**, 8350 (2014).
9. X. Wang, Z. Cheng, K. Xu, H. K. Tsang, and J.-B. Xu, Nat. Photonics **7**, 888 (2013).
10. K. Kim, J. Choi, T. Kim, S. Cho, and H. Chung, Nature **479**, 338 (2011).
11. M. A. Gluba, D. Amkreutz, G. V. Troppenz, J. Rappich, and N. H. Nickel, Appl. Phys. Lett. **103**, 073102 (2013).
12. E. D. Palik, *Handbook of Optical Constants of Solids* (Academic, 1985).
13. W. Gao, J. Shu, C. Qiu, and Q. Xu, ACS Nano **6**, 7806 (2012).
14. J. Tao, X. Yu, B. Hu, A. Dubrovkin, and Q. J. Wang, Opt. Lett. **39**, 271 (2014).
15. I. Arrazola, R. Hillenbrand, and A. Y. Nikitin, Appl. Phys. Lett. **104**, 011111 (2014).
16. D. J. Bergman, Phys. Rep. **43**, 377 (1978).
17. X.-T. Kong, X. Yang, Z. Li, Q. Dai, and X. Qiu, Opt. Lett. **39**, 1345 (2014).
18. K. S. Novoselov, A. K. Geim, S. V. Morozov, D. Jiang, Y. Zhang, S. V. Dubonos, I. V. Grigorieva, and A. A. Firsov, Science **306**, 666 (2004).
19. A. Satou, Y. Koseki, V. Ryzhii, V. Vyurkov, and T. Otsuji, J. Appl. Phys. **115**, 104501 (2014).